Modelling Diffraction by Facetted Particles

E. Hesse[a,*], A. Macke[b], S. Havemann[c], A.J. Baran[c], Z. Ulanowski[a], P.H. Kaye[a]

[a]*University of Hertfordshire, Centre for Atmospheric and Instrumentation Research, Hatfield, Hertfordshire AL10 9AB, UK*

[b]*Leibniz-Institut für Troposphärenforschung e.V., Permoserstraße 15 04318 Leipzig, Germany*

[c] *Met Office, Cordonan 2, Fitzroy Road, Exeter, EX13 PB, UK*

Abstract

A method to approximate azimuthally resolved light scattering patterns and phase functions due to diffraction and external reflection by strongly absorbing facetted particles is demonstrated for a cube and compared with results from an exact method, T-matrix. A phase function averaged over a range of orientations of a strongly absorbing hexagonal column of aspect ratio unity has been calculated and tested against Discrete Dipole Approximation (DDA) results for a size parameter of 50.

Keywords: diffraction; facetted particle; Kirchhoff approximation; light scattering

* Corresponding author. Tel.: +441707286170; fax: +441707284185.
E-mail address: e.hesse@herts.ac.uk (E.Hesse).

1. Introduction

Airborne particles such as ice crystals [1] and Saharan dust [2] influence the Earth-Atmosphere radiation balance by scattering and absorbing solar radiation. To be able to understand the radiative transfer properties of such particles, a detailed knowledge of their shapes and sizes is required. Imaging methods, e.g. [3], are widely used to obtain in situ morphological data of atmospheric particles. However, for small particles, optical aberrations, and constrained depth of field restrict the obtainable information. Such constrains do not apply to the detection of scattering patterns. Therefore, suitable detection instruments like the Small Ice Detector (SID) [4] have been developed. However, while conventional pattern recognition methods may be readily used to group recorded images into broad particle shape classes, the inversion of the patterns required to yield quantitative morphological data is much more involved. Therefore, the creation of data bases of scattering patterns of known particle morphologies is extremely useful for particle classification.

Computations of light-scattering properties for non-axisymmetric particles based on exact methods like the T-matrix [5,6] and discrete dipole approximation (DDA) [7] have upper size parameter limits of applicability, depending on particle shape and complex refractive index. For moderate values of the size parameter $2\pi a/\lambda$, where a is a characteristic length of the particle and λ the wavelength, the finite difference time domain (FDTD) method can be used [8], but it places too severe demands on computational resources. Thus, despite its limitations, geometric optics and/or physical optics is still the most widely used model for moderate to large size parameters.

In the classical geometric optics approximation scattered light is divided into two parts, firstly light reflected or transmitted by the scatterer, and secondly externally diffracted light. Improved methods to combine the ray-tracing and diffraction parts have been presented by Muinonen [9] and Yang and Liou [10] and Bi et al. [11]. However, computational methods, which calculate the ray-tracing and diffraction contributions separately, are still widely used. In many geometric optics ray tracing codes, e.g. [12-14], external diffraction is approximated by Fraunhofer diffraction on the projected cross section, applying Babinet's principle. Macke et al. [12,13] have used the Kirchhoff approximation to model diffraction by polygonal apertures corresponding to the projected particle cross section. The calculation of diffraction by a circular aperture at oblique incidence by means of the Kirchhoff approximation is described in [15]. Here, this method is extended to oblique incidence on polygonal apertures. Furthermore, it is investigated, if diffraction by facetted particles can be modelled by superposing the diffraction patterns of individual incident light facing facets. As a test, the far field diffraction pattern caused by an arrangement of apertures corresponding to the facets of a cube is calculated and compared with the T-matrix result [16] for a strongly absorbing cube ($n = 1.5 + i0.2$). The high imaginary part has been chosen in order to keep the amount of transmitted light negligible. In order to improve the approximation, the same diffraction procedure has been applied to externally reflected light. As a further test, the averaged phase function for a set of orientations of a hexagonal column is compared with DDA results for a size parameter of 50 given in [11].

2. Diffraction by oblique apertures

Using Kirchhoff's diffraction theory, the diffracted field amplitudes for distances between a plane scattering surface S and the observer large compared to the wavelength of the incident light can be approximated as follows [15]:

$$\vec{\mathbf{E}}(\vec{\mathbf{x}}) = \frac{ie^{ikr}}{2\pi r}\vec{\mathbf{k}} \times \int_S \vec{\mathbf{n}} \times \vec{\mathbf{E}}(\mathbf{x}')e^{i\vec{\mathbf{k}}\vec{\mathbf{x}}'}da' \tag{1}$$

where $k = 2\pi/\lambda$ is the wave number, $\vec{\mathbf{x}}'$ is the coordinate of the element of surface area da', $\vec{\mathbf{n}}$ is the unit surface normal in positive z'-direction, r is the length of the vector $\vec{\mathbf{x}}$ from the origin to the observation point, and $\vec{\mathbf{k}}$ is the normalized wave vector in the direction of observation.

We consider a plane wave with wave vector $\vec{\mathbf{k}}_0$ incident at an angle α on a thin, perfectly conducting screen with a polygonal opening situated in the $x'y'$ plane (Fig. 1). The plane of incidence is chosen to be the $x'z'$ plane. The unit vectors in the x', y' and z'directions are $\vec{\epsilon_1}$, $\vec{\epsilon_2}$ and $\vec{\epsilon_3}$, respectively. Since the wave is incident from the right, $z' < 0$ is the region of diffraction fields. The two components of the incident wave polarized parallel and perpendicular to the scattering plane can be treated separately: the component of the electric field parallel to the plane of incidence is

$$\vec{\mathbf{E}}_{i\parallel} = E_{0\parallel}(\vec{\epsilon_1}\cos\alpha - \vec{\epsilon_3}\sin\alpha)e^{ik(z'\cos\alpha + x'\sin\alpha)} \tag{2a}$$

The exact field in the surface integral is approximated by the incident field:

$$\left(\vec{\mathbf{n}} \times \vec{\mathbf{E}_{i\parallel}}\right)_{z'=0} = E_{0\parallel}\vec{\epsilon_2}\cos\alpha\, e^{ik\sin\alpha\, x'} \tag{3a}$$

Inserting Eq. (3a) into Eq. (1) gives

$$\vec{E}_{\parallel x'z'}(\vec{\mathbf{x}}) = \frac{ie^{ikr}E_{0\parallel}\cos\alpha}{2\pi r}\left(\vec{\mathbf{k}} \times \vec{\epsilon_2}\right)\int_S e^{ik\sin\alpha x'}\, e^{i\left(k_x x' + k_y y'\right)}dx'dy' \tag{4a}$$

The components of $\vec{\mathbf{k}}$ can be expressed in polar coordinates: $k_x = \cos\varphi'\sin\theta'$; $k_y = \sin\varphi'\sin\theta'$; $k_z = \cos\theta'$.

$$\begin{aligned}\vec{E}_{\parallel x'z'}(\vec{\mathbf{x}}) &= \frac{ie^{ikr}E_{0\parallel}\cos\alpha}{2\pi r}\left(\vec{\mathbf{k}} \times \vec{\epsilon_2}\right)\int_S e^{ik[x'(\sin\alpha + \cos\varphi'\sin\vartheta') + y'(\sin\varphi'\sin\vartheta')}\, dx'dy' \\ &= \frac{ie^{ikr}E_{0\parallel}\cos\alpha}{2\pi r}\left(\vec{\mathbf{k}} \times \vec{\epsilon_2}\right)F(\mathrm{S}, \alpha; \vartheta', \varphi')\end{aligned} \tag{5a}$$

The component of the incident electric field perpendicular to the plane of incidence is

$$\vec{\mathbf{E}}_{i\perp} = E_{0\perp}\vec{\epsilon_2}e^{ik(z'\cos\alpha + x'\sin\alpha)} \tag{2b}$$

Again, the exact field in the surface integral is approximated by the incident field:

$$\left(\vec{\mathbf{n}} \times \vec{\mathbf{E}_{i\perp}}\right)_{z'=0} = -E_{0\perp}\vec{\epsilon_1}e^{ik(x'\sin\alpha)} \tag{3b}$$

Inserting Eq. (3b) into Eq. (1) gives the scattered field component parallel to the $y'z'$-plane as,

$$\vec{E}_{\parallel y'z'}(\vec{\mathbf{x}}) = -\frac{ie^{ikr}E_{0\perp}}{2\pi r}\left(\vec{\mathbf{k}} \times \vec{\epsilon_1}\right)\int_S e^{ikx'\sin\alpha}\, e^{i\left(k_x x' + k_y y'\right)}dx'dy' \tag{4b}$$

$$\vec{E}_{\parallel y'z'}(\vec{\mathbf{x}}) = -\frac{ie^{ikr}E_{0\perp}}{2\pi r}\left(\vec{\mathbf{k}} \times \vec{\epsilon_1}\right)F(\mathrm{S}, \alpha; \vartheta', \varphi') \tag{5b}$$

In the following we use $E_{\|x'z'}(\vec{\mathbf{x}})$ and $E_{\|y'z'}(\vec{\mathbf{x}})$ as approximations for the magnitude of the electric field components parallel and perpendicular to the incidence plane. In order to be able to add diffraction contributions from different apertures, we rotate the Jones vector into the scattering plane defined by the vectors $\vec{\mathbf{k}}$ and $\vec{\mathbf{k}}_0$ using the formalism described by Hovenier and Mee [17]. The surface integral $F\left(S,\alpha;\vartheta',\varphi'\right)$ in Eq. (5b) is the same as in Eq. (5a). It can be evaluated using Green's theorem [12,13]:

$$\begin{aligned}\int_S e^{ik\left[x'\left(\sin\alpha+\cos\varphi'\sin\vartheta'\right)+y'\sin\varphi'\sin\vartheta'\right]}dx'\,dy' \\ = -\oint_S \frac{e^{ik\left[x'\left(\sin\alpha+\cos\varphi'\sin\vartheta'\right)+y'\sin\varphi'\sin\vartheta'\right]}}{2ik\sin\varphi'\sin\vartheta'}dx' \\ +\oint_S \frac{e^{ik\left[x'\left(\sin\alpha+\cos\varphi'\sin\vartheta'\right)+y'\sin\varphi'\sin\vartheta'\right]}}{2ik\left(\sin\alpha+\cos\varphi'\sin\vartheta'\right)}dy'\end{aligned} \tag{6}$$

where the line integrals are along the boundary of the aperture.

For an aperture of polygonal shape the boundary is defined by its vertices p_1, p_2, ..., p_{n+1} with $p_{n+1} = p_1$. Therefore, the line integral in eq. (6) can be expressed as a sum of integrals along straight lines. With

$$y'(x') = y'_{p_j} + \frac{y'_{p_{j+1}} - y'_{p_j}}{x'_{p_{j+1}} - x'_{p_j}}\left(x' - x'_{p_j}\right) \tag{7}$$

we obtain for the contribution between p_j and p_{j+1} to the first and second line integral on the right hand side of eq.(6)

$$\begin{aligned}-\int_{p_j}^{p_{j+1}} \frac{e^{ik\left[x'\left(\sin\alpha+\cos\varphi'\sin\vartheta'\right)+y'\sin\varphi'\sin\vartheta'\right]}}{2ik\sin\varphi'\sin\vartheta'}dx' \\ = \frac{x_{p_{j+1}} - x_{p_j}}{2k^2\sin\varphi'\sin\vartheta'\left[\left(x_{p_{j+1}} - x_{p_j}\right)\left(\sin\alpha+\cos\varphi'\sin\vartheta'\right)+\left(y_{p_{j+1}} - y_{p_j}\right)\sin\varphi'\sin\vartheta'\right]}\times \\ \times\left(e^{\left\{ik\left[x_{p_{j+1}}\left(\sin\alpha+\cos\varphi'\sin\vartheta'\right)+y_{p_{j+1}}\sin\varphi'\sin\vartheta'\right]\right\}} - e^{\left\{ik\left[x_{p_j}\left(\sin\alpha+\cos\varphi'\sin\vartheta'\right)+y_{p_j}\sin\varphi'\sin\vartheta'\right]\right\}}\right)\end{aligned} \tag{8}$$

$$\begin{aligned}\int_{p_j}^{p_{j+1}} \frac{e^{ik\left[x'\left(\sin\alpha+\cos\varphi'\sin\vartheta'\right)+y'\sin\varphi'\sin\vartheta'\right]}}{2ik\left(\sin\alpha+\cos\varphi'\sin\vartheta'\right)}dy' \\ = \frac{y_{p_{j+1}} - y_{p_j}}{2k^2\left(\sin\alpha+\cos\varphi'\sin\vartheta'\right)\left[\left(x_{p_{j+1}} - x_{p_j}\right)\left(\sin\alpha+\cos\varphi'\sin\vartheta'\right)+\left(y_{p_{j+1}} - y_{p_j}\right)\sin\varphi'\sin\vartheta'\right]}\times \\ \times\left(e^{\left\{ik\left[x_{p_{j+1}}\left(\sin\alpha+\cos\varphi'\sin\vartheta'\right)+y_{p_{j+1}}\sin\varphi'\sin\vartheta'\right]\right\}} - e^{\left\{ik\left[x_{p_j}\left(\sin\alpha+\cos\varphi'\sin\vartheta'\right)+y_{p_j}\sin\varphi'\sin\vartheta'\right]\right\}}\right)\end{aligned} \tag{9}$$

From this follows

$$\int_S e^{ik\left[x'\left(\sin\alpha+\cos\varphi'\sin\vartheta'\right)+y'\sin\varphi'\sin\vartheta'\right]}dx'\,dy' =$$

$$= \frac{1}{2k^2}\sum_{j=1}^{n}\left(e^{\left\{ik\left[x_{p_{j+1}}\left(\sin\alpha+\cos\varphi'\sin\vartheta'\right)+y_{p_{j+1}}\sin\varphi'\sin\vartheta'\right]\right\}}-e^{\left\{ik\left[x_{p_j}\left(\sin\alpha+\cos\varphi'\sin\vartheta'\right)+y_{p_j}\sin\varphi'\sin\vartheta'\right]\right\}}\right)\times \quad (10)$$

$$\times\frac{\left(x_{p_{j+1}}-x_{p_j}\right)/\left(\sin\varphi'\sin\vartheta'\right)-\left(y_{p_{j+1}}-y_{p_j}\right)/\left(\sin\alpha+\cos\varphi'\sin\vartheta'\right)}{\left(x_{p_{j+1}}-x_{p_j}\right)\left(\sin\alpha+\cos\varphi'\sin\vartheta'\right)+\left(y_{p_{j+1}}-y_{p_j}\right)\sin\varphi'\sin\vartheta'}$$

The approximations for the two components of the electric field $\overrightarrow{E_{\parallel}}(\vec{\mathbf{x}})$ and $\overrightarrow{E_{\perp}}(\vec{\mathbf{x}})$ at position $\vec{\mathbf{x}}$ can now be calculated by combining Eqs. (5a) and (5b) with Eq. (10), respectively. The intensity of the scattered light at position $\vec{\mathbf{x}}$ is proportional to $\vec{\mathbf{E}}(\vec{\mathbf{x}})\cdot\vec{\mathbf{E}}^{*}(\vec{\mathbf{x}})$.

The angles θ' and φ' are defined with respect to the aperture coordinate system *x'y'z'* (Fig. 1). The *z*-axis of the original coordinate system is parallel to the direction of propagation $\overrightarrow{\mathbf{k_0}}$ of the incident ray but has opposite direction. In order to obtain the electric field in direction [θ, φ] at a distance *R* large compared to the wavelength, we calculate the coordinates [*x*,*y*,*z*] corresponding to this position. Then two coordinate system transformations are performed, starting with the [*x*,*y*,*z*] system: First, a rotation about the *z*-axis, so that the new axis y^{*} is parallel to $\overrightarrow{\mathbf{k_0}}\times\vec{\mathbf{n}}$, and after that a rotation about the y^{*}-axis by $\arccos\left(\overrightarrow{\mathbf{k_0}}\cdot\vec{\mathbf{n}}\right)$, resulting in the new axis *z'* being parallel to $\vec{\mathbf{n}}$. Next, the electric field components can be calculated in the *x'y'z'* coordinate system using Eqs. (5a), (5b) and (10). Finally, the electric field components are expressed with respect to the scattering plane.

Eqs. (5) were derived for the hemisphere on the side of the aperture facing away from the light source. In order to be able to calculate diffraction for the opposite hemisphere too, we multiply the equation by the obliquity factor (cos(**n**,**r**)-cos(**n**,**ρ**))/2 derived for an unobstructed spherical wave originating at a point source [18], see Fig. 2. The unit vectors **n**, **r** and **ρ** are the outward facing surface normal at the surface point considered, the vector pointing from the point at which the disturbance shall be calculated towards the centre of the surface element considered, and the vector pointing from the source to the centre of the surface element, respectively. In our case, the light incident on the facetted particle is parallel. This means that the source is far away, and **ρ** is equal to the propagation vector of the incident light. Since the integral of the incident field over the surface of the scattering particle is zero, we need only to consider either the part of the particle surface facing towards or away from the source when calculating diffraction.

3. Approximation of external diffraction and reflection by strongly absorbing facetted objects

In the following we investigate if the above method can be applied to an arrangement of flat apertures, or facets of a scattering object, in order to estimate the intensity distribution of light diffracted around and reflected by the scatterer. The example of a strongly absorbing cube will be discussed. Results for a hexagonal column will also be presented.

First, a cube with an edge length *a* equal to 3.676 times the wavelength λ and refractive index $n = 1.5 + 0.2i$ is considered. The high imaginary part was chosen in order to minimize contributions from refracted light to the scattering pattern. The cube is positioned in such a way that two facets are illuminated by the incident light. They are aligned symmetrically with respect to the direction of incidence, which is perpendicular to the edge closest to the light source (see inset of Fig. 4).

Fig. 3 shows the scattering pattern in polar coordinates calculated by an exact method, T-matrix [16] (fifth column) together with results for three different aperture arrangements. The first column in Fig. 3 corresponds to diffraction on the projected cross section. It is commonly used to calculate the contribution of diffraction to scattering in geometric optics ray-tracing codes (e.g. [12-14]). However, in this approach it is wrongly assumed that the propagation direction of the incident wave would be parallel to the normals of the facets containing the edges contributing to the contour of the projected cross section. To correct this, diffraction by two apertures sized and aligned like the incident wave facing facets 1 and 2 in the inset of Fig. 4 has been calculated (second column). In the third column external reflection has been added. In the fourth column the very small diffraction contributions due to the two facets parallel to the incident direction have been included.

The azimuthally resolved diffraction patterns are presented in three different logarithmic scales: four and a half decades (first row), seven decades (second row) and ten decades (third and fourth row). The upper three rows show the polar diffraction patterns for zenith angles $0° \leq \theta \leq 90°$, and the fourth row for $90° \leq \theta \leq 180°$. At the lowest dynamic sensitivity, the results for all calculation methods look similar, showing the zeroth and first order diffraction maxima corresponding to Fraunhofer diffraction at a rectangular aperture. In the intermediate dynamic range, diffraction by the projected cross section looks still like a reasonably good approximation; however its intensity decays more slowly with increasing scattering angle in the vertical direction in Fig.3, corresponding to $\varphi = 90°$ and $\varphi = 270°$. The result for two oblique apertures shown in the second column of Fig.3 is a better approximation. Adding external reflection by the two facets results in the two spots around $[\theta = 90°; \varphi = 0°]$ and $[\theta = 90°; \varphi = 180°]$.

For the highest considered dynamic sensitivity the scattering patterns for diffraction by the projected cross section and T-matrix look very different. The first shows one vertical branch, whereas in the latter two vertical arcs occur. Interestingly, adding the small diffraction contributions from the two facets parallel to the incident light to the scattering patterns in column 3 increases the similarity of the scattering pattern with the T-matrix result. The corresponding phase functions averaged over azimuth angles (φ was varied in 1° steps) are presented in Fig. 4.

As a further test we compare the averaged phase function for a set of orientations of a hexagonal column with DDA results [11]. The column has a diameter to height ratio of one to one and a refractive index of $1.3+0.1i$. The size parameter in terms of column height is 50. The phase function has been averaged over ten orientations in 10° intervals starting with the cylinder axis perpendicular to the direction of propagation of the incident light and two symmetrically aligned illuminated facets. The cylinder is then rotated around an axis through the centre of gravity, which is perpendicular to the cylinder axis and perpendicular to the propagation direction of the incident light (see inset of Fig. 5). The DDA results can be found in [11] and those of the method described here in Fig.5. The phase functions agree well.

Apart from practical applications, this multi-aperture diffraction approach can help our understanding of the diffraction process: the most important features are the contour of the particle and the size of the projected area. They determine the position of the lower order diffraction maxima. If high dynamic sensitivity is considered, the spatial alignment of the facets contributing to the diffraction process becomes important: oblique incidence results in curved diffraction arcs, and even facets perpendicular to the direction of the incident light contribute to the light scattering pattern.

4. Summary

In many geometric optics ray tracing codes, e.g. [12-14], external diffraction is approximated by Fraunhofer diffraction on the projected cross section by applying Babinet's principle. Macke

[12,13] employed the Kirchhoff approximation to model diffraction by polygonal apertures at perpendicular incidence. Here, this method has been extended. Diffraction by polygonal apertures is calculated using the correct incidence angles. Furthermore, externally reflected light is modelled as undergoing diffraction in the same way as light incident in the direction of the reflected geometric optics ray from inside the crystal would be. As a test, the far field light scattering pattern caused by an arrangement of apertures corresponding to the incident-wave facing facets of a cube has been compared with the T-matrix result [16] for the case of strong absorption. It has been found that light scattering patterns calculated using this new approach represent typical features like arcs, which cannot be modelled via diffraction on the projected cross section. Therefore, the presented computational method may become a useful tool for the generation of reference databases of scattering patterns for interpretation of data measured by probes like SID. Additionally to the azimuthally resolved scattering patterns, phase functions have been compared with T-matrix and DDA results.

References

[1] Baran A. A review of the light scattering properties of cirrus. JQSRT 2009;110: 1239–1260.

[2] Yu H, Kaufman YJ, Chin M, Feingold G, Remer LA, Anderson TL, et al. A review of measurement-based assessments of the aerosol direct radiative effect and forcing. Atmos. Chem. Phys. 2006;6:613-66.

[3] Lawson RP, Korolev AV, Cober SG, Huang T, Strapp JW, Isaac GA. Improved measurements of the drop size distribution of a freezing drizzle event. Atmos. Res. 1998;48:181-91.

[4] Kaye PH, Hirst E, Greenaway RS et al. Classifying atmospheric ice crystals by spatial light scattering. Opt. Lett. 2008;33:1545-47.

[5] Mishchenko MI, Videen G, Babenko VA, Khlebtsov NG, Wriedt T. T-matrix theory of electromagnetic scattering by particles and itsapplications: a comprehensive reference database. JQSRT 2004;88:357–406.

[6] Mishchenko MI, Videen G, Babenko VA, Khlebtsov NG, Wriedt T. Comprehensive T-matrix reference database: a 2004–06 update. JQSRT 2007;106:304–24.

[7] Yurkin MA, Maltsev VP, Hoekstra AG. The discrete dipole approximation: an overview and recent developments. JQSRT 2007;106:558–89.

[8] Yang P, Liou KN. In: Mishchenko MI, Hovenier JW, Travis LD, editors. Light scattering by nonspherical particles. New York: Academic Press; 1999. p. 173–221.

[9] Muinonen K. Scattering of light by crystals: a modified Kirchhoff approximation. Appl Opt 1989;28:3044–50.

[10] Yang P, Liou KN. Geometric-optics-integral equation method for light scattering by nonspherical ice crystals. Appl Opt 1996;35:6568–84.

[11] Bi L, Yang P, Kattawar GW, Hu Y, Baum BA. Scattering and absorption of light by ice particles: Solution by a new physical-geometric optics hybrid method. JQSRT 2011;1492-1508.

[12] Macke A, Mueller J, Raschke E. Single scattering properties of atmospheric ice crystals. J Atmos Sci 1996;53:2813–25.

[13] Macke A. Modellierung der optischen Eigenschaften von Cirruswolken. PhD thesis, University of Hamburg, Germany; 1994.

[14] Hesse E, Mc Call DS, Ulanowski Z, Stopford C, Kaye PH. Application of RTDF to particles with curved surfaces. JQSRT 2009;1599-1603.

[15] Jackson JD. Classical Electrodynamics. 3rd ed. John Wiley & Sons, New York 1999, chapter 10.9.

[16] Havemann S, Baran AJ. Extension of *T*-matrix to scattering of electromagnetic plane waves by non-axisymmetric dielectric particles: application to hexagonal ice cylinders. JQSRT 2001;70:139-158.
[17] Hovenier JW, Mee CVM. Fundamental relationships relevant to the transfer of polarized light in a scattering atmosphere. Astron. Astrophys. 1983;128:1-16.
[18] Hecht E. Optics. 4th ed. Addison Wesley, San Francisco 2002, chapter 10.4.

Captions of Figures

Fig. 1: Diffraction by an aperture: oblique incidence.

Fig. 2: Vectors used for the calculation of the obliquity factor. Points S and P correspond to the point source and the observation point, respectively.

Fig. 3: Comparison of the polar scattering pattern of a cube (a = 3.676λ; n=1.5+0.2i; for orientation see inset of Fig. 4) calculated using the T-matrix method (fifth column) with results for different aperture arrangements: projected cross section (first column), diffraction by two apertures aligned as facets 1 and 2 (second column), diffraction and reflection by facets 1 and 2 (third column) and diffraction by facets 3 and 4 added to diffraction and reflection by facets 1 and 2 (fourth column). The comparisons are given for three different logarithmic scales: 4.5 decades (first row), 7 decades (second row) and 10 decades (third and fourth row). Light scattering into the forward hemisphere is shown, except for the fourth row, which shows the back-facing hemisphere.

Fig. 4: Comparison of the azimuthally averaged phase function calculated using the T-matrix method with results for different aperture arrangements: projected cross section, two apertures aligned as facets 1 and 2 in Fig. 2, and a four-aperture arrangement (see text).

Fig. 5: Averaged phase function for a set of orientations (see text) of a hexagonal column of diameter to height ratio one. The size parameter in terms of height is 50 and n=1.3+0.1i.

Fig. 1

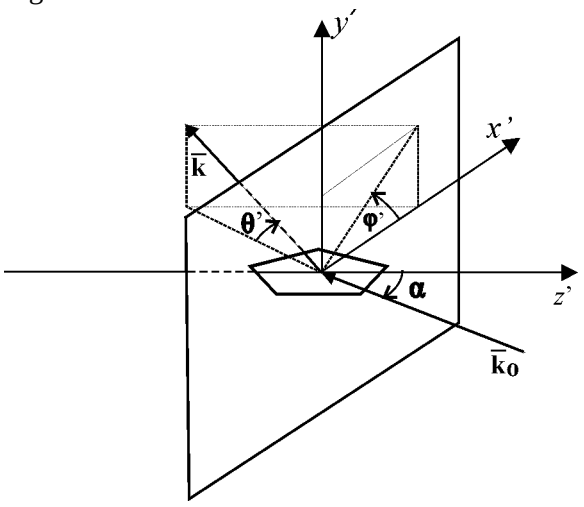

Fig. 2

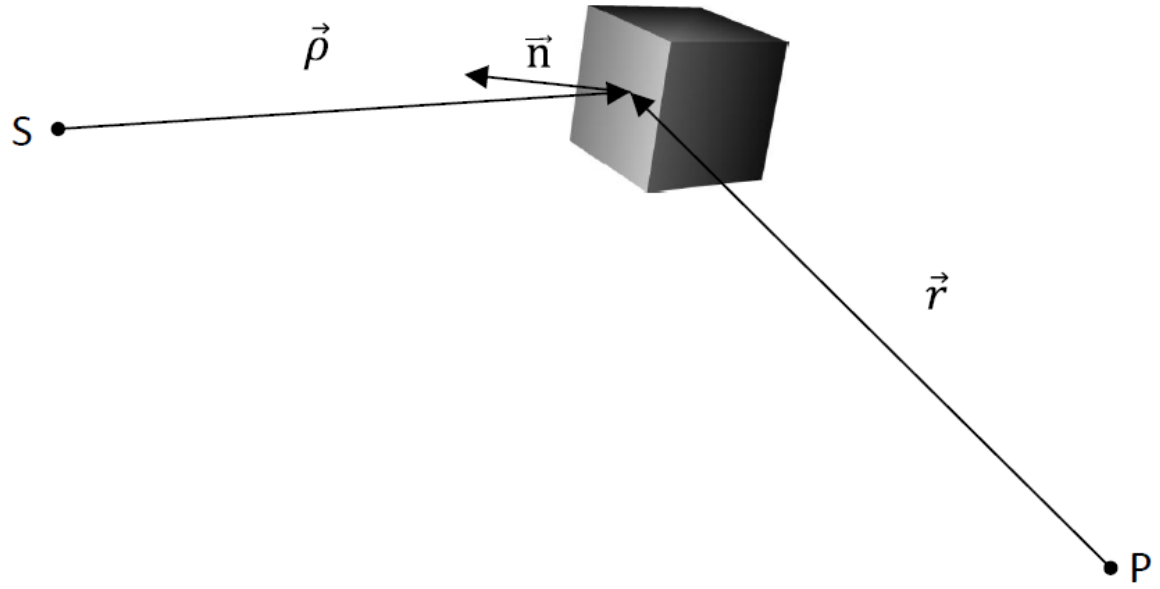

Fig. 3

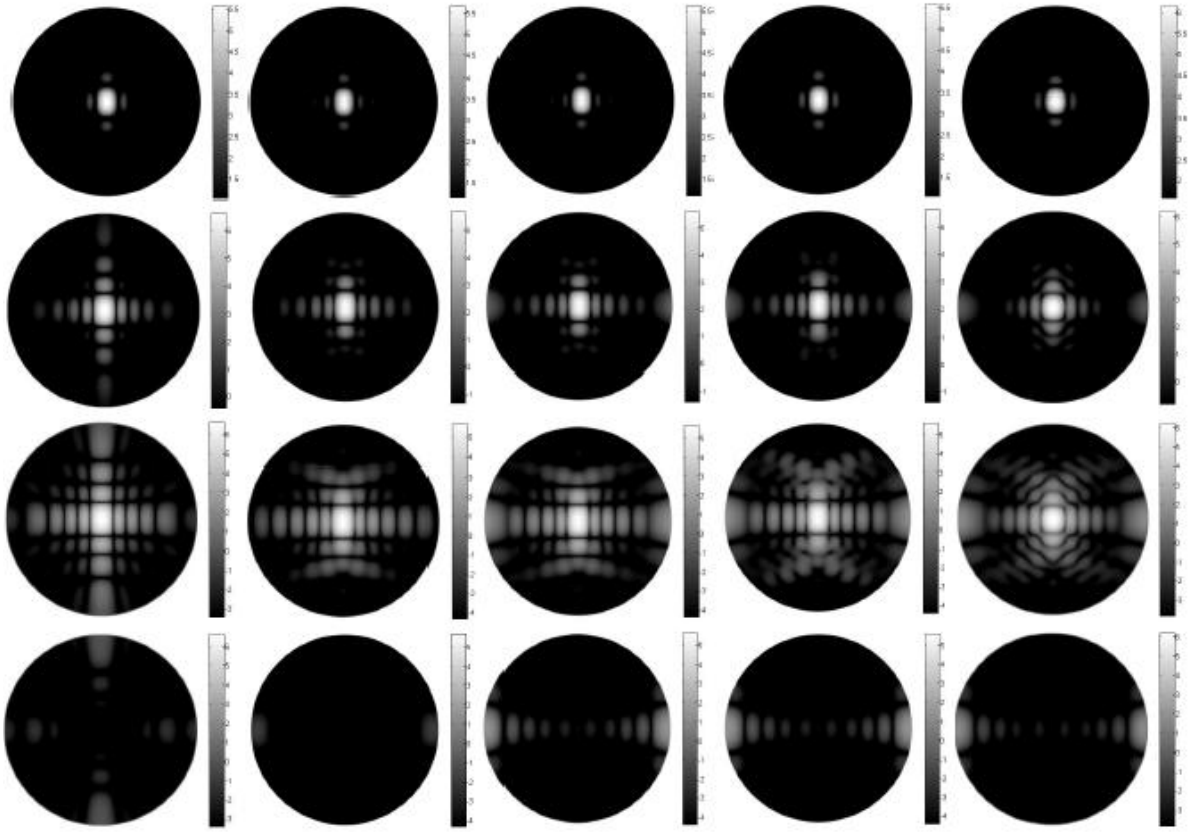

Fig. 4

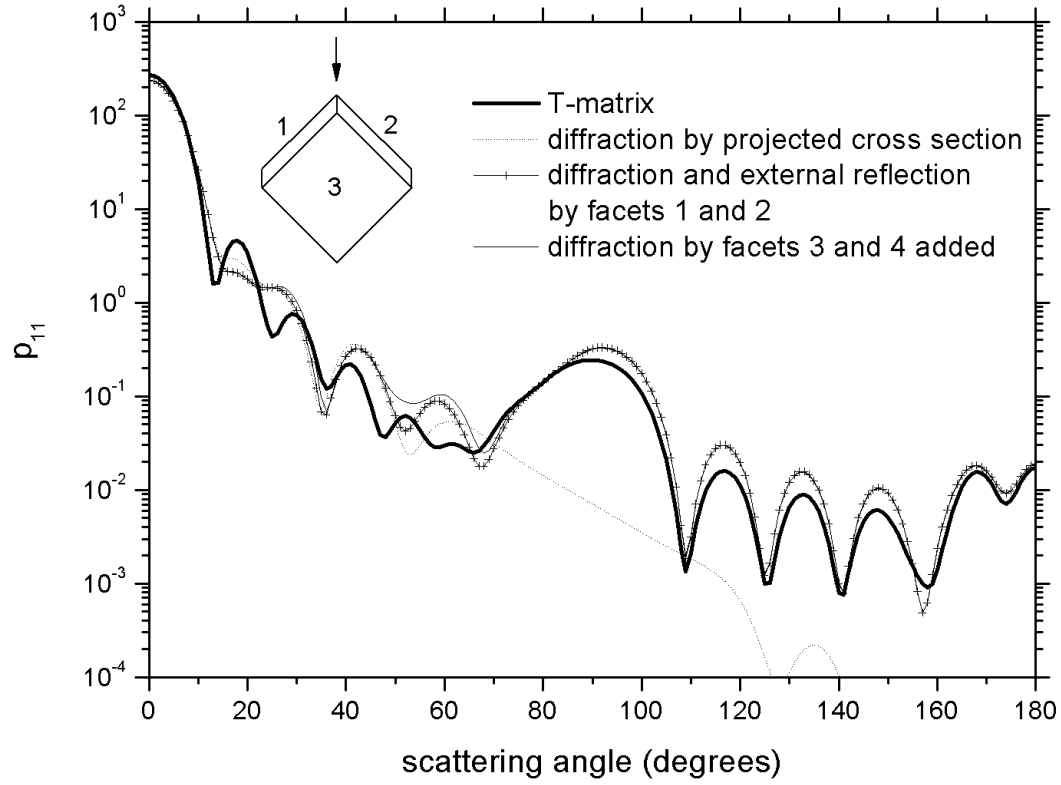
T-matrix
diffraction by projected cross section
diffraction and external reflection
by facets 1 and 2
diffraction by facets 3 and 4 added
1
2
3
p11
scattering angle (degrees)

Fig. 5

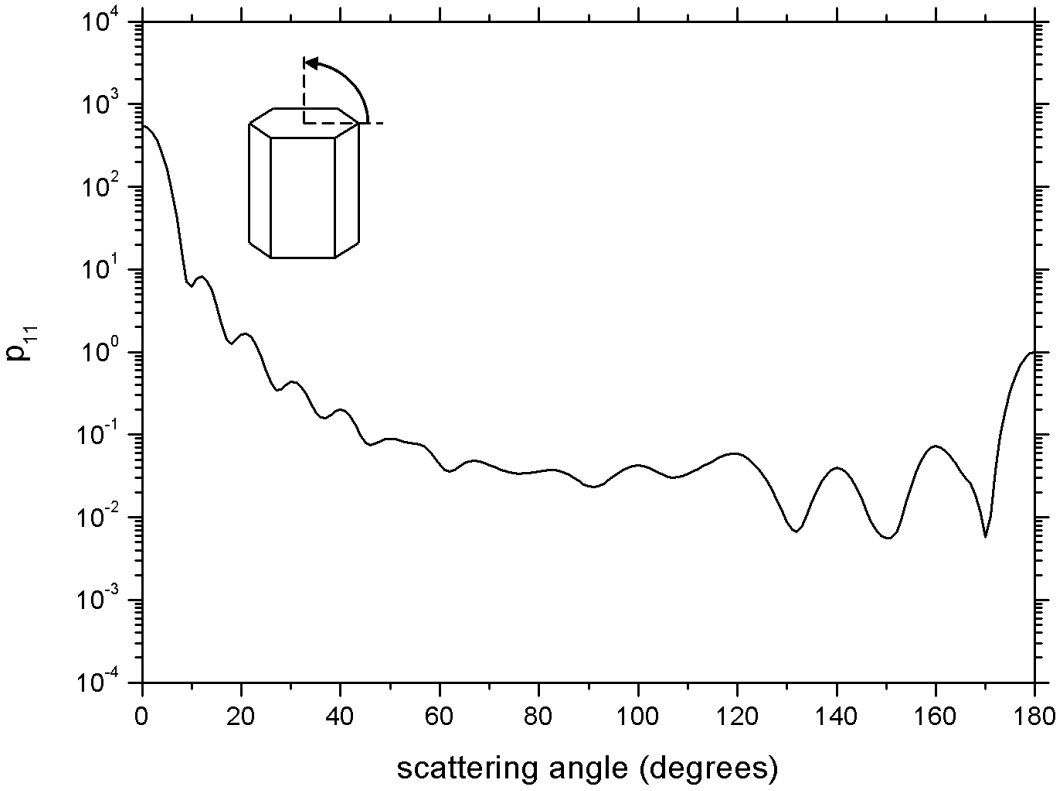
p11
scattering angle (degrees)